Journal of The Electrochemical Society, **158** (5) A585-A591 (2011)
0013-4651/2011/158(5)/A585/7/$28.00 © The Electrochemical Society

Reversible Insertion of a Trivalent Cation onto MnO_2 Leading to Enhanced Capacitance

Prasant Kumar Nayak and N. Munichandraiah[*,z]

Department of Inorganic and Physical Chemistry, Indian Institute of Science, Bangalore 560012, India

Supercapacitor properties of MnO_2 are studied generally in aqueous alkali metal salt solutions, often in a Na salt solution. During electrochemical discharge-charge processes, Na^+ ions from the electrolyte get reversibly inserted/deinserted on the surface of MnO_2 particles, which leads to redox reaction between MnOONa and MnO_2. In the present study, it has been shown that MnO_2 exhibits enhanced capacitance behaviour in a rare earth metal salt solution, namely, $La(NO_3)_3$ solution in comparison with $NaNO_3$ and $Mg(NO_3)_2$ aqueous solutions. The specific capacitance increases with an increase in charge on the solution cation (Na^+, Mg^{2+} and La^{3+}). It is proposed that the number of surface sites for adsorption of cations remains unaltered in all solutions. The surface insertion of cation facilitates the reduction of Mn^{4+} in MnO_2 to Mn^{3+} equivalent to the charge present on the cation. As the specific capacitance is related to the quantity of charge that is exchanged between the solid MnO_2 and the aqueous solution, the trivalent cation (La^{3+}) provides greater specific capacitance than in $Mg(NO_3)_2$ and $NaNO_3$ electrolytes. Accordingly, the number of Mn(IV)/Mn(III) redox pairs involved in the neighbourhood of the adsorption site is one, two and three when Na^+, Mg^{2+} and La^{3+} ions, respectively, are adsorbed.

Manuscript submitted November 18, 2010; revised manuscript received February 15, 2011. Published March 28, 2011.

Manganese oxides have been under intense investigations for electrochemical energy storage and conversion because of their high electrochemical activity, variable oxidation states, low cost and environmental compatibility.[1–3] MnO_2 is useful for electrochemical supercapacitors,[4] which are expected to meet high pulse power demands. MnO_2 is generally studied for its capacitance properties in neutral aqueous solutions of an alkali salt, for instance Na_2SO_4.[4–7] When a MnO_2 electrode is subjected to discharge in Na_2SO_4 electrolyte, reduction of Mn^{4+} to Mn^{3+} occurs with a simultaneous insertion of Na^+ ion onto the oxide surface leading to the formation of MnOONa. Non-diffusive reversible transitions of surface $MnO_2 \leftrightarrow$ MnOONa are responsible for providing charge in pseudo-capacitance properties.[7–9] It has been established that the crystallographic structures of MnO_2 which possess sufficient gap or interlayer distance (α- and δ- MnO_2) are appropriate for insertion of Na^+ ions into them.[9] Although the theoretical specific capacitance (SC) of MnO_2, on the basis of reduction of Mn^{4+} to Mn^{3+}, is 1100 F g^{-1} over a potential window of 1.0 V, in practice this value is never realized for MnO_2 powders. However, SC values equal to the theoretical value was reported for a MnO_2 thin film electrode.[7] A value of 470 F g^{-1} is reported for nanocomposites consisting of several oxides of Mn.[10] Nevertheless, for electrodes employing MnO_2 powders, experimental results from various laboratories indicate values of SC in a range from 100 to 250 F g^{-1}.[11–13] The wide range of SC values are due to differences in methods of synthesis of MnO_2, crystallographic structures, morphology, particle size, porosity, loading of MnO_2 on the substrate current collectors, methods of measurement (cyclic voltammetry or galvanostatic charge-discharge cycling), sweep rates used in cyclic voltammetry, current density (or specific current, A g^{-1}) used in galvanostatic charge-discharge cycling, etc. Nevertheless, it is noted that the maximum value of SC reported is only about 30% of the theoretical value, assuming that the manganese oxide is present as MnO_2. Recently, it was reported that the specific capacitance of MnO_2 in Ca and Mg salt solution is greater than that in Na salt solutions.[14,15]

The aim of the present investigation is to study the insertion of a rare earth metal trivalent cation, namely, La^{3+} onto MnO_2. Interestingly, the specific capacitance measured in a La salt solution is greater than the values measured in Na and Mg salt solutions under similar experimental conditions.

Experimental

Nano-structured MnO_2 was prepared by reduction of $KMnO_4$ with ethylene glycol.[16] In a typical preparation, 0.1 M of $KMnO_4$ (3.16 g) was dissolved in 200 mL of doubly distilled water and then 5 mL of ethylene glycol was slowly added to the above solution under stirring at ambient environment. The stirring was continued for 3 h to ensure the completion of reaction. The resulting black precipitate was filtered and washed with distilled water several times followed by ethanol and dried in air at 60°C for overnight.

Powder X-ray diffraction (XRD) pattern of MnO_2 was recorded on a Bruker D8 Advance X-ray diffractometer using Cu Kα ($\lambda = 1.5418$ Å) as the source. Raman scattering spectrum of MnO_2 was collected by HORIBA Jobin Yvon Lab RAM HR100 Raman instrument using argon ion laser of wavelength 514 nm. The morphology of MnO_2 sample was examined by a FEI Co. scanning electron microscope (SEM) model Sirion. The Brunauer-Emmet-Teller (BET) surface area measurement was carried out using Micromeritics surface area analyzer model ASAP 2020. X-ray photoelectron spectroscopy (XPS) studies were conducted with XPS Thermo Fisher Scientific, UK using X-ray Al anode (monochromatic Kα X-rays at 1486.6 eV) as the source. The C 1S region was used as the reference and was set at 284.6 eV.

For electrochemical characterization, electrodes were fabricated on a high purity grade 304 stainless steel (SS) foil (thickness: 0.2 mm) as the current collector. For this, the SS was polished with successive grades of emery and washed thoroughly with detergent, etched in dilute HCl, rinsed with doubly distilled water and then with acetone, and dried in air. MnO_2 (70 wt %), Ketjen black EC-600 JD (Akzo Noble Polymer Chemicals) (20 wt %) and poly(vinylidene fluoride) (Aldrich) (10 wt %) were mixed and ground in a mortar. Several drops of n-methyl pyrrolidinone (Aldrich) were added to make a syrup, which was coated on the pre-treated SS foil of 1.0 cm^2 area and dried at 100°C under vacuum for 12 h. Coating and drying steps were repeated to get a loading level of 0.5–0.6 mg cm^{-2}. A Mettler Toledo electronic balance model AB265-S/FACT with 0.01 mg sensitivity was used for weighing the electrodes. The electrochemical studies were performed in a glass cell of about 50 mL volume, which had provision to introduce MnO_2 coated SS as the working electrode, Pt foil as the counter electrode and saturated calomel electrode (SCE) as the reference electrode. The aqueous electrolytes investigated include $NaNO_3$, $Mg(NO_3)_2$ and $La(NO_3)_3$. The concentration of each electrolyte was 0.1 M. The specific conductivity values measured in 0.1 M solutions of $NaNO_3$, $Mg(NO_3)_2$ and $La(NO_3)_3$ were 0.011, 0.018 and 0.025 Ohm^{-1} cm^{-1}, respectively. An Eco Chemie potentiostat/galvanostat model Autolab PGSTAT 30 was used for all the electrochemical studies. Potential

---

[*] Electrochemical Society Active Member.
[z] E-mail: muni@ipc.iisc.ernet.in

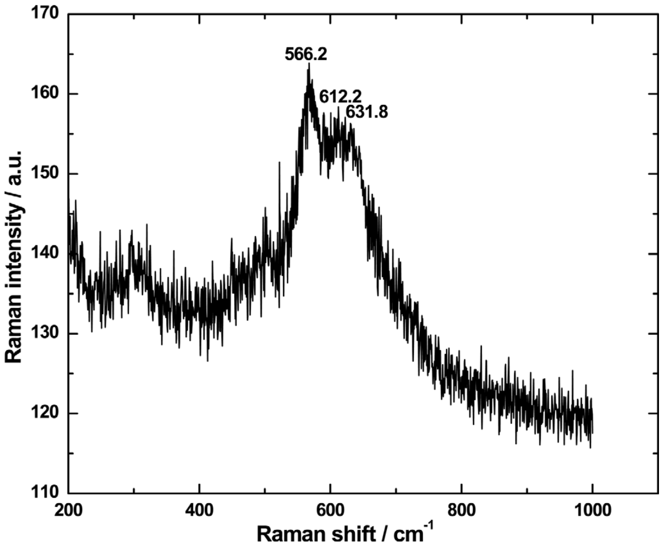

Figure 1. Raman spectrum of MnO_2.

values were reported with respect to SCE. All experiments were conducted in an air-conditioned room at 22 ± 1°C.

Results and Discussion

Powder XRD pattern of MnO_2 indicated that MnO_2 is mainly in amorphous state with a broad prominent peak at $2\theta = 14°$ and another small peak at $2\theta = 30°$, as reported previously.[16] These two peaks indicated that the sample is δ-MnO_2. The broad peaks indicated nano-particle nature of the sample. It is understood that the sample has short-range δ-type structure although it is nearly X-ray amorphous.[16] δ-MnO_2 is a 2D layered compound with the interlayer distance of 7.0 Å.[9] The Raman scattering spectrum shown in Fig. 1 is characterized by peaks at 566.2, 612.2 and 631.8 cm^{-1}. These peaks are mainly attributed to the stretching vibrations of MnO_6 octahedra.[17] In SEM micrograph of MnO_2 powder (Fig. 2), nearly spherical nano-particles with diameter in the range 20–50 nm were observed. The N_2 adsorption-desorption isotherm is shown in Fig. 3. A hysteresis loop of IV type at p/p^o between 0.70 and 0.99 is observed, suggesting the existence of mesopores in the particles. The BET surface area measured in the range $p/p^o = 0.05$–0.25 was 212 m^2 g^{-1}.

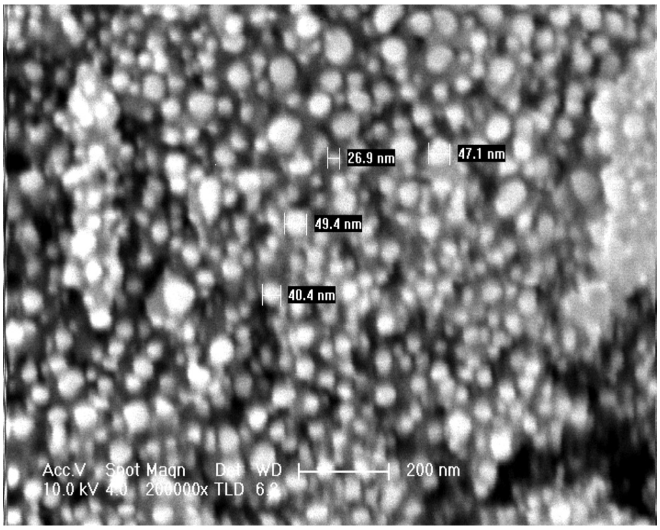

Figure 2. SEM micrograph of MnO_2.

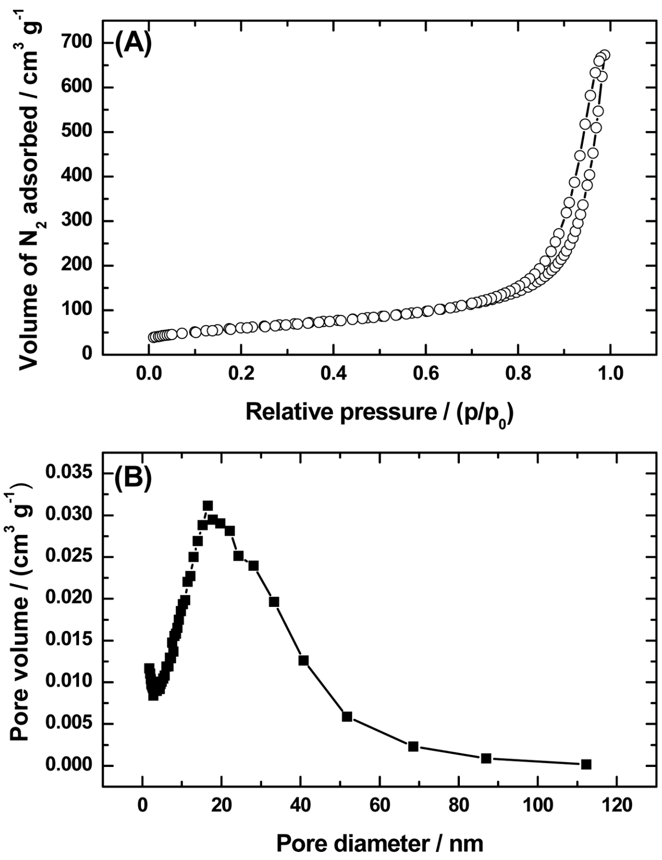

Figure 3. (A) N_2 adsorption-desorption isotherm and (B) pore size distribution of MnO_2.

Using the MnO_2 coated stainless steel electrodes, electrochemical studies were carried out in 0.1 M aqueous electrolytes of $NaNO_3$, $Mg(NO_3)_2$ and $La(NO_3)_3$ under identical conditions. Although it is known that the potential window appropriate for MnO_2 to exhibit capacitance behaviour in Na_2SO_4 electrolyte is 0.0–1.0 V, it is intended to examine the effect of the nature of the electrolyte on potential window. Typical voltammograms recorded at a sweep rate of 10 mV s^{-1} are presented in Fig. 4. In Na_2SO_4 electrolyte (Fig. 4A), when the potential range is −1.0 to 1.4 V (curve i), multiple current peaks are observed in both cathodic and anodic scans. Current tends to increase at −1.0 V due to hydrogen evolution reaction (HER). The increasing current at about 1.2 V is due to oxygen evolution reaction (OER). When MnO_2 electrode is cycled between −0.5 and 1.4 V in Na_2SO_4 electrolyte (Fig. 4A, curve ii) and also between 0.0 and 1.4 V (curve iii), current peaks appear. However, if the potential range is limited from 0.0 to 1.0 V (curve iv), the voltammogram tends to become rectangular in shape, which is an indication for the capacitance behaviour of MnO_2. In $Mg(NO_3)_2$ and $La(NO_3)_3$ electrolytes, the voltammograms (Figs. 4B and 4C) recorded in the potential ranges between −1.0 and 1.4 V; −0.5 and 1.4 V; and 0.0 and 1.4 V (curves i, ii and iii) consist of current peaks similar to the observations made in Na_2SO_4 (Fig. 4A). However, the potential range where MnO_2 shows rectangular shape of cyclic voltammograms in $Mg(NO_3)_2$ and $La(NO_3)_3$ is limited between 0.2 and 1.0 V. Voltammograms were recorded at different sweep rates varying from 5 to 50 mV s^{-1} in the potential range of 0.2–1.0 V in 0.1 M aqueous electrolytes of $NaNO_3$, $Mg(NO_3)_2$ and $La(NO_3)_3$, and are shown in Fig. 5. At all sweep rates, the voltammograms exhibit rectangular shape, suggesting capacitance behaviour of MnO_2 in all electrolytes.

Typical charge-discharge curves of MnO_2 electrodes at a current density (c.d.) of 0.5 mA cm^{-2} (1.0 A g^{-1}) in the potential range of 0.0–1.0 V in aqueous electrolytes of $NaNO_3$, $Mg(NO_3)_2$ and

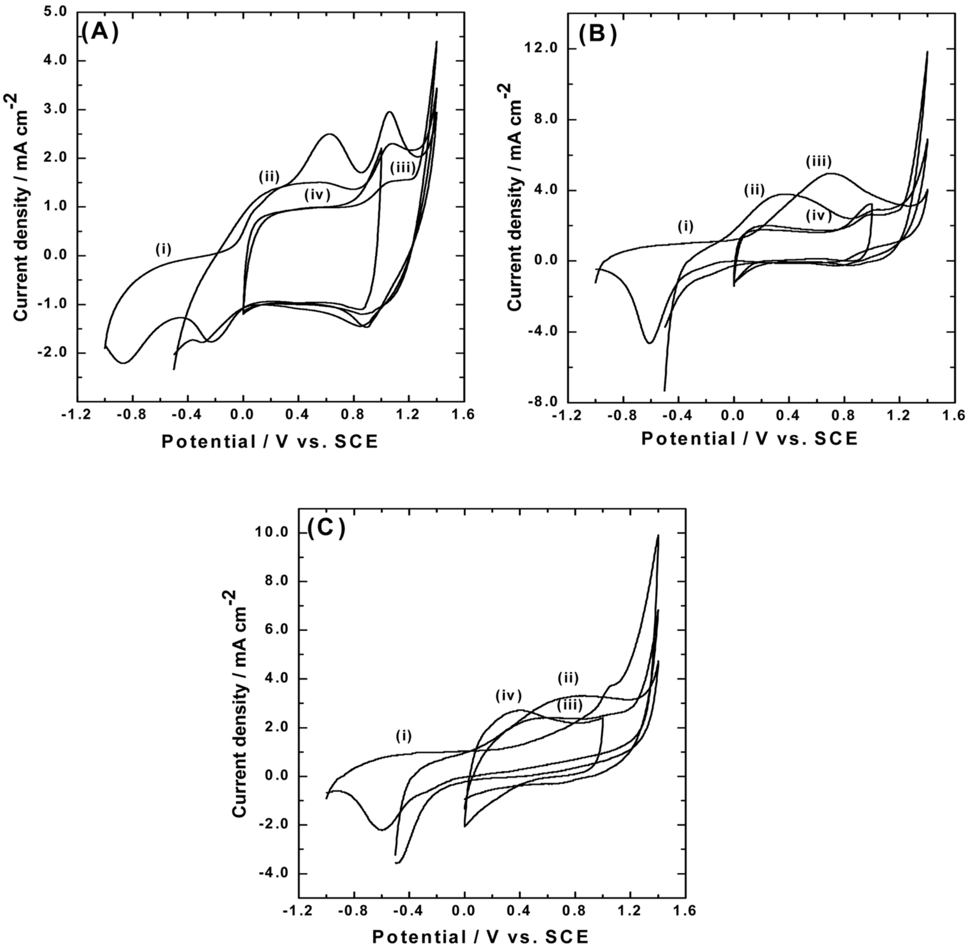

Figure 4. Cyclic voltammograms at a sweep rate of 10 mV s^{-1} in different potential ranges of (i) −1.0 to 1.4 V, (ii) −0.5 to 1.4 V, (iii) 0.0–1.4 V and (iv) 0.0–1.0 V in 0.1 M aqueous electrolytes of (A) $NaNO_3$, (B) $Mg(NO_3)_2$ and (C) $La(NO_3)_3$.

$La(NO_3)_3$ are shown in Fig. 6. There is a linear variation of potential with time in $NaNO_3$ electrolyte during charging and discharging processes. However, in $Mg(NO_3)_2$ and $La(NO_3)_3$ electrolytes, the variation of potential with time is linear in the potential range of 0.2–1.0 V. A plateau-like behaviour is observed in the potential range between 0.2 and 0.0 V, which is also reflected in cyclic voltammograms. The plateau-like behaviour during discharge of the MnO_2 electrode between 0.2 and 0.0 V is attributed to diffusion controlled battery-like property in $Mg(NO_3)_2$ and $La(NO_3)_3$ electrolytes. Thus, capacitor behaviour in 1.0–0.2 V range and battery behaviour in 0.2–0.0 are observed in $Mg(NO_3)_2$ and $La(NO_3)_3$ electrolytes, although capacitor behaviour is observed in 1.0–0.0 V range in $NaNO_3$ electrolyte. Therefore, further charge-discharge studies were carried out in 0.2–1.0 V range in all electrolytes for the purpose of comparison. Charge-discharge data recorded for a few cycles in $NaNO_3$, $Mg(NO_3)_2$ and $La(NO_3)_3$ electrolytes in 0.2–1.0 V range are presented in Fig. 7. The discharge SC of MnO_2 was calculated using the following equation

$$\mathrm{SC} = \mathrm{I}\,\mathrm{t}/(\Delta\mathrm{E}\ \mathrm{m}) \qquad [1]$$

where I is the charge-discharge current, m is the mass of MnO_2 present in the electrode and t is the discharge time corresponding to the voltage window, ΔE (= 0.8 V). The SC values of MnO_2 electrodes obtained at a c.d. of 0.5 mA cm^{-2} (1.0 A g^{-1}) are 187, 211 and 257 F g^{-1} in $NaNO_3$, $Mg(NO_3)_2$ and $La(NO_3)_3$ electrolytes, respectively.

Recent studies of Xu et al, on capacitance properties of MnO_2 involve aqueous electrolytes of Mg^{2+}, Ca^{2+} and Ba^{2+} ions over a potential window of 0.9 V.[14,15] Under similar experimental conditions, MnO_2 provided SC values of 320 and 194 F g^{-1} in $Ca(NO_3)_2$ and $NaNO_3$ electrolytes, respectively. The higher specific capacitance of MnO_2 in $Ca(NO_3)_2$ solution than in $NaNO_3$ electrolyte was attributed to divalent cationic species.[14] Asymmetric capacitors of activated carbon/MnO_2 were studied in $Mg(NO_3)_2$, $Ca(NO_3)_2$ and $Ba(NO_3)_2$ electrolytes.[15] $Mg(NO_3)_2$ and $Ca(NO_3)_2$ electrolytes were assessed to be better electrolytes than $NaNO_3$ and $Ba(NO_3)_2$ electrolytes. The results of the present work in $NaNO_3$ and $Mg(NO_3)_2$ electrolytes agree well with the results reported earlier,[15] although the actual values of specific capacitance show some difference. The values of SC depend on several experimental conditions such as the amount of active material per unit area, potential window, current density used for charge-discharge cycling or sweep rate used for cyclic voltammetry, etc., which are different in the present work as compared with the previous reports.[14,15] Nevertheless, the trend in variation of SC with the Na^+ and Mg^{2+}- solutions is essentially the same to a previous report.[15] In addition to the above two cations, the present study involves La^{3+} ion. SC of MnO_2 measured in $La(NO_3)_3$ is found to be greater than the values measured in both $NaNaO_3$ and $Mg(NO_3)_2$ electrolytes.

The charge storage mechanism of MnO_2 is scarcely discussed in the literature.[7–9] The capacitance behaviour of MnO_2 is known due to reversible redox process involving Mn^{4+}/Mn^{3+} in the solid MnO_2 followed by insertion/deinsertion of cations

$$\mathrm{nMnO_2} + \mathrm{M^{n+}} + \mathrm{ne^-} \leftrightarrow (\mathrm{MnOO})_n\mathrm{M} \qquad [2]$$

where M^{n+} represents the cation. While this reaction is expected to take place on or near surface region of MnO_2 particles, it is also reported by Kuo and Wu that bulk insertion/extraction of H_3O^+ occurs into/from a crystalline structure of electrochemically deposited MnO_2.[6] In the present study, as the oxide is mainly amorphous with short range crystallinity, it is likely that the insertion of cations

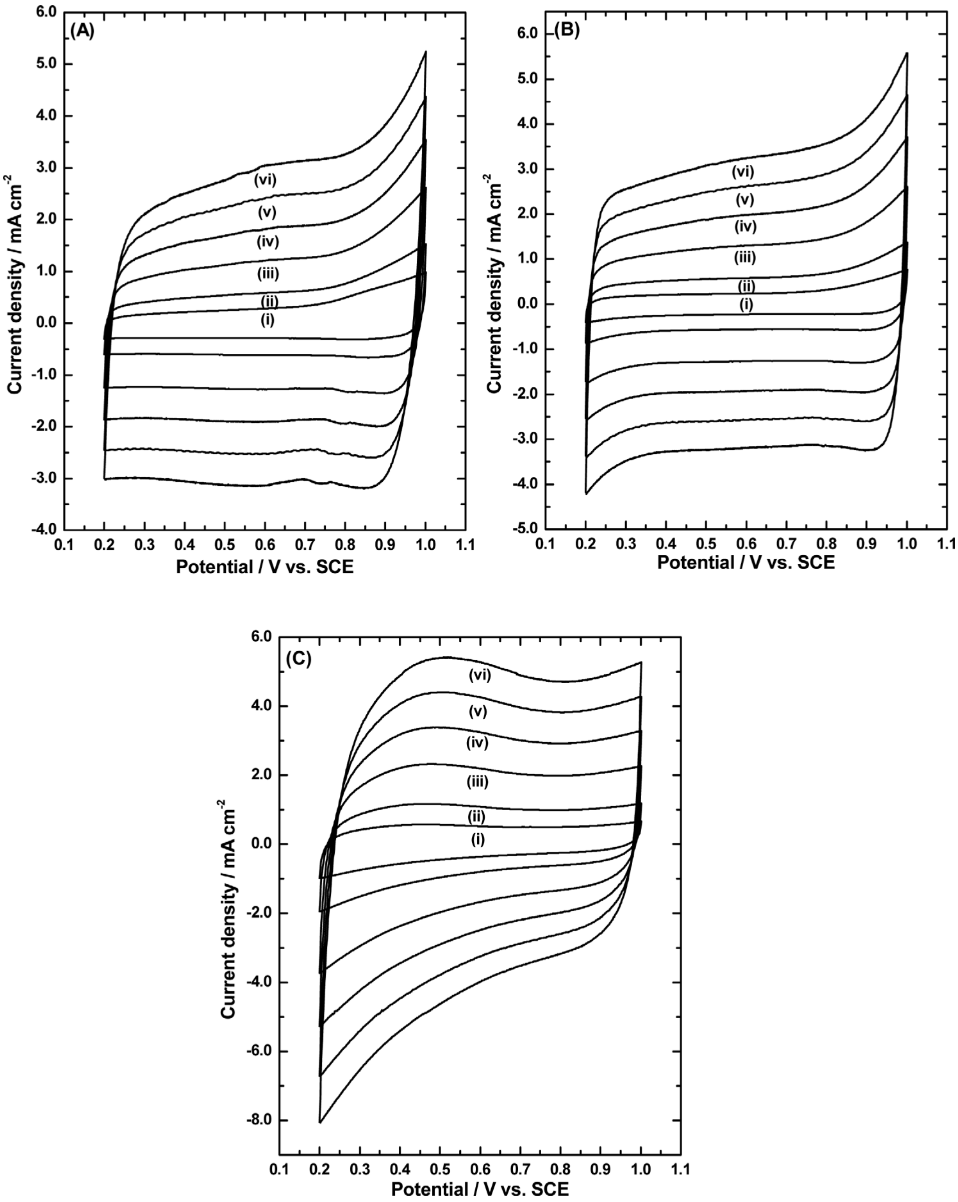

Figure 5. Cyclic voltammograms at sweep rates of (i) 5, (ii) 10, (iii) 20, (iv) 30, (v) 40 and (vi) 50 mV s^{-1} in the potential range from 0.2 to 1.0 V in 0.1 M aqueous electrolytes of (A) $NaNO_3$, (B) $Mg(NO_3)_2$ and (C) $La(NO_3)_3$.

takes place predominantly at the surface of the MnO_2 particles.[11] This means, the cations entering the oxide particle concentrate on the surface and they do not diffuse into the bulk of the particle. This assumption is supported by the fact that the SC reported for MnO_2 so far in the literature is substantially lower than the theoretical value. Values of SC close to the theoretical value could have been obtained if bulk MnO_2 particles involve in the redox process. Assuming that the number of adsorption sites available for cation insertion remains the same irrespective of the valency of the cations, the positive charge of the inserted cation is double in the case of divalent cation and triple in the case of trivalent cation when compared with monovalent cation. Accordingly, the amount of Mn^{4+} getting reduced to Mn^{3+} in the solid becomes double and triple in the neighbourhood of adsorption site when divalent and trivalent cations get inserted in comparison with monovalent cation. Hence, the value of SC in divalent cation and trivalent cation electrolytes is expected to be double and triple, respectively to the value in monovalent cation electrolyte. However, it is seen that there is a substantial increase in SC of MnO_2 in $Mg(NO_3)_2$ electrolyte, but it is not double to the SC measured in $NaNO_3$ electrolyte. The differences in SC of MnO_2 in electrolytes of different cations may be attributed to

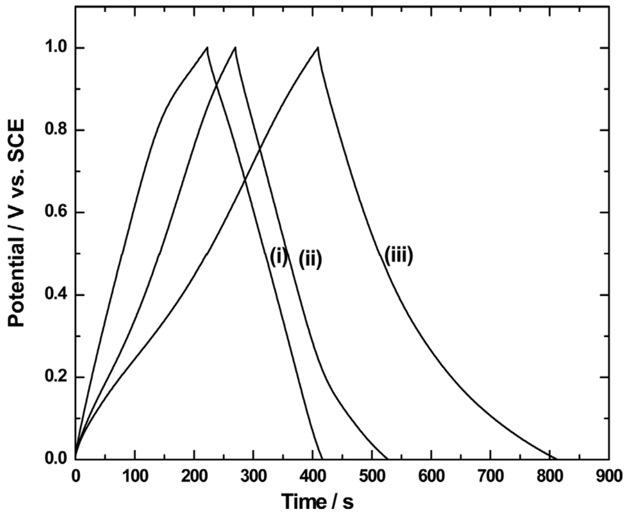

Figure 6. Charge-discharge cycle of MnO_2 at a c.d. of 0.5 mA cm^{-2} (1.0 A g^{-1}) in the potential range of 0.0–1.0 V in 0.1 M aqueous electrolytes of (i) $NaNO_3$, (ii) $Mg(NO_3)_2$ and (iii) $La(NO_3)_3$.

differences in size of cations. Effective ionic radii of Na^+, Mg^{2+} and La^{3+} in aqueous solutions are 4, 8 and 9 Å, respectively.[18] The ionic conductivity of the electrolyte is not expected to play a role in the specific capacitance, and the three electrolytes used in the present study have nearly the same specific conductivity (see Experimental section). Nevertheless, it is interesting to note that MnO_2 exhibits capacitance behaviour in an aqueous electrolyte containing the trivalent ion, La^{3+} with increased SC in comparison with monovalent and divalent cations. A schematic picture of surface insertion of different valency cations and reduction of Mn^{4+} to Mn^{3+} in MnO_2 is shown in Fig. 8.

In order to identify the presence of the trivalent cation (La^{3+}) in MnO_2 after insertion into it, a MnO_2 electrode was galvanostatically discharged to 0.0 V and was held at this potential for 24 h, subsequently removed, washed, dried and subjected for recording of XPS spectrum. As shown in Fig. 9, La is identified.[19] This data confirms that the La^{3+} ion gets inserted on to the surface of MnO_2 particles.

The charge-discharge cyclings of MnO_2 electrodes were carried out at different current densities in the potential range from 0.2 to 1.0 V in the three electrolytes. The SC values obtained using Eq. 1 are plotted against the charge-discharge c.d. and shown in Fig. 10. In general, there is a decrease in SC with an increase in c.d. in all electrolytes. However, a higher SC is obtained in aqueous

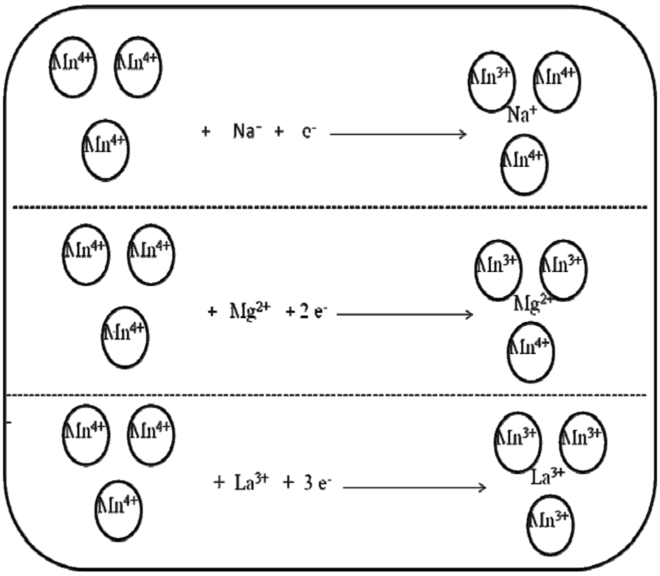

Figure 8. Schematic picture of surface insertion of cations, Na^+, Mg^{2+} and La^{3+} followed by reduction of Mn^{4+} to Mn^{3+} on MnO_2 particles.

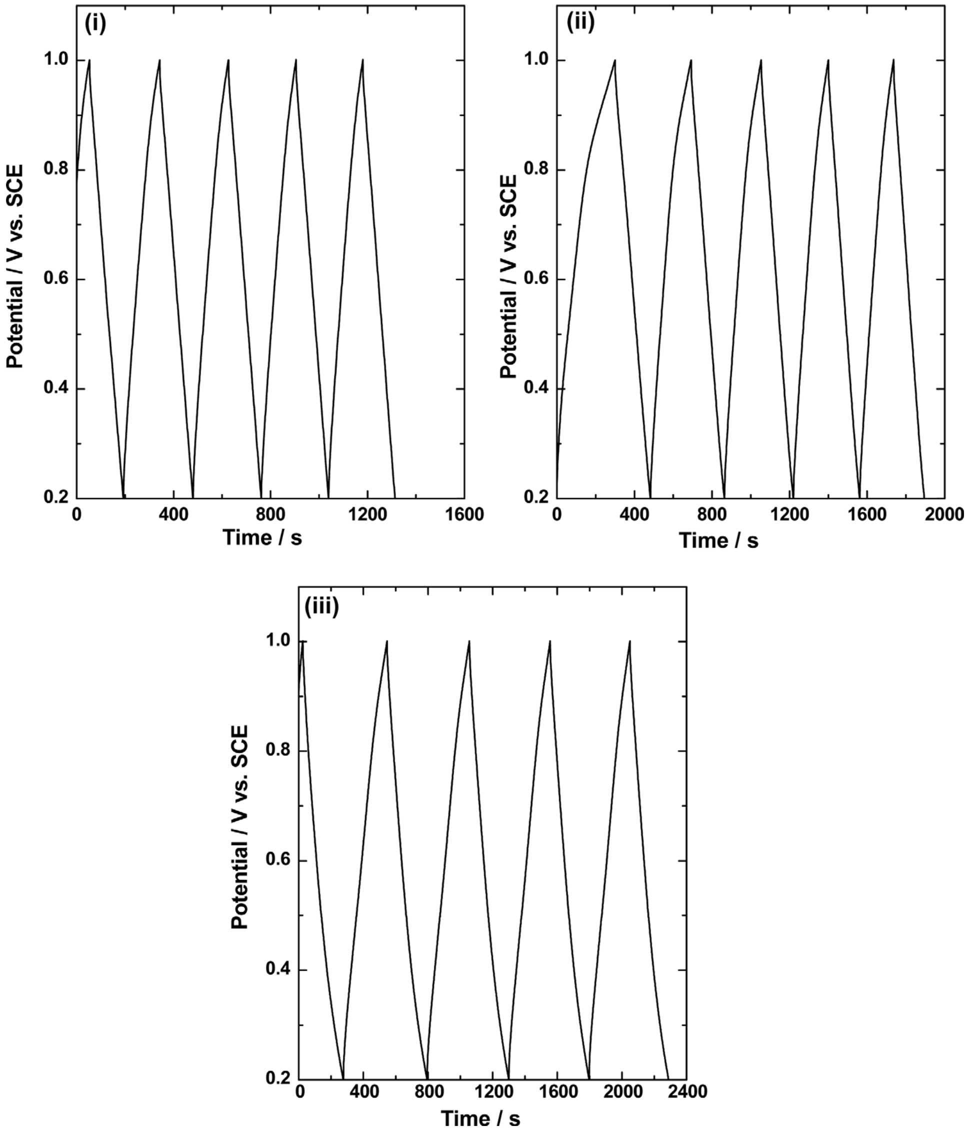

Figure 7. Charge-discharge cycling of MnO_2 at a c.d. of 0.5 mA cm^{-2} (1.0 A g^{-1}) in the potential range from 0.2 to 1.0 V in 0.1 M aqueous electrolytes of (i) $NaNO_3$, (ii) $Mg(NO_3)_2$ and (iii) $La(NO_3)_3$.

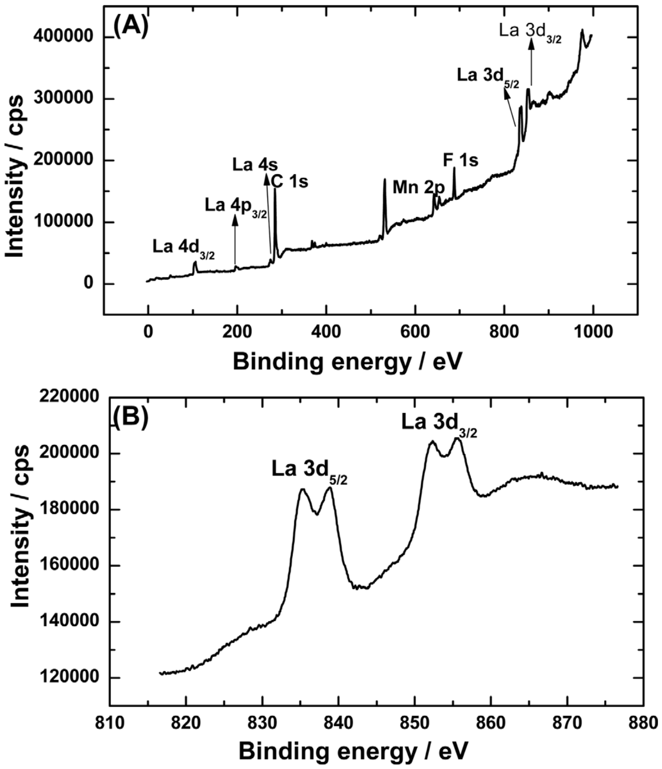

Figure 9. (A) XPS spectrum showing the presence of La on MnO_2 and (B) the expanded 3d energy level of La.

electrolyte of $La(NO_3)_3$ in comparison to aqueous electrolytes of $NaNO_3$ and $Mg(NO_3)_2$ at all charge-discharge c.d.s from 0.5 to 20.0 mA cm^{-2} (1.0–40.0 A g^{-1}). Thus, it is shown in the present work that in addition to the insertion of alkali and alkaline earth cations in MnO_2, La^{3+} ions can also be inserted. The reversible insertion/deinsertion of La^{3+} ions results in an increased specific capacitance of MnO_2.

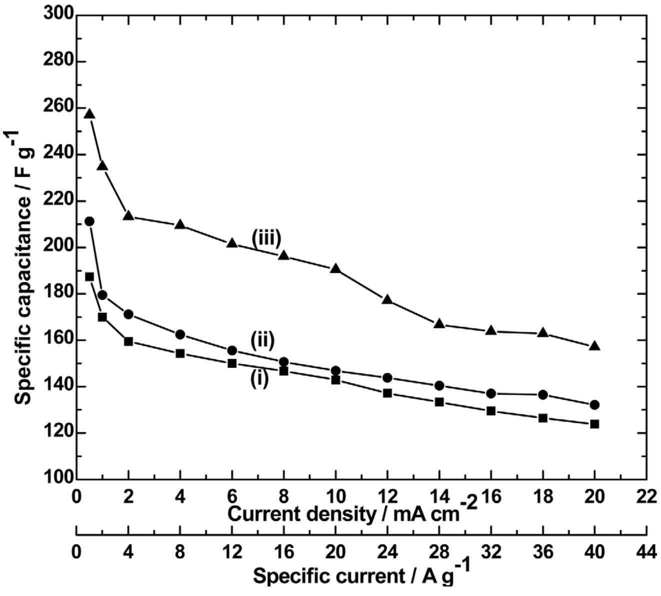

Figure 10. Variation of specific capacitance of MnO_2 with charge-discharge current density in 0.1 M aqueous electrolytes of (i) $NaNO_3$, (ii) $Mg(NO_3)_2$ and (iii) $La(NO_3)_3$ in potential window from 0.2 to 1.0 V.

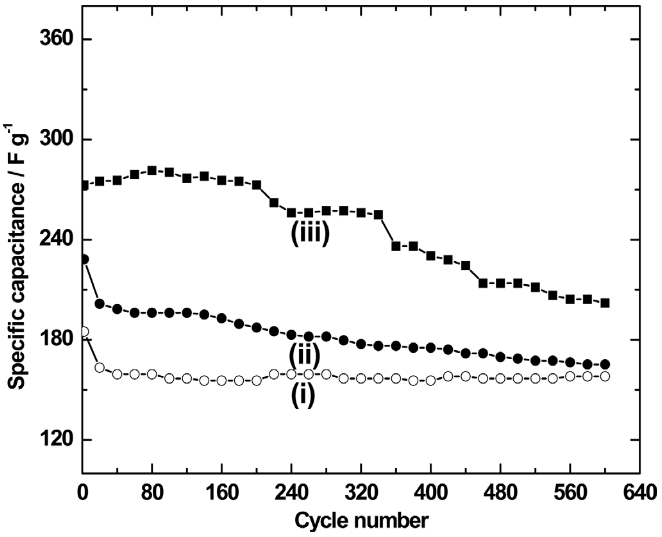

Figure 11. Cycle life test of MnO_2 at a charge-discharge c.d. of 0.5 mA cm^{-2} (1.0 A g^{-1}) in 0.1 M aqueous electrolytes of (i) $NaNO_3$, (ii) $Mg(NO_3)_2$ and (iii) $La(NO_3)_3$ in the potential window from 0.2 to 1.0 V.

The cycle-life of MnO_2 electrodes were tested by galvanostatic charge-discharge cycling at a current density of 0.5 mA cm^{-2} (1.0 A g^{-1}) in the potential range of 0.2–1.0 V in all the three electrolytes (Fig. 11). In $NaNO_3$, an initial discharge SC of 185 F g^{-1} is obtained, which decreases to 163 F g^{-1} after 20 cycles. Then the SC becomes stabilized and a discharge SC of 160 F g^{-1} is obtained after 600 cycles. In $Mg(NO_3)_2$, an initial discharge SC of 228 F g^{-1} is obtained, which rapidly falls to a value of 202 F g^{-1} after 20 cycles. Then it slowly decreases and a discharge SC of 166 F g^{-1} is obtained after 600 cycles. In $La(NO_3)_3$, an initial discharge SC of 272 F g^{-1} is obtained, which slowly increases to a value of 281 F g^{-1} for first 100 cycles. Then it starts to decrease slowly and a SC of 202 F g^{-1} is obtained after 600 cycles. Thus the SC obtained after 600 cycles in $La(NO_3)_3$ is greater in comparison to that in $NaNO_3$ and $Mg(NO_3)_2$ electrolytes. There are about 13, 27 and 26% decrease in SC in $NaNO_3$, $Mg(NO_3)_2$ and $La(NO_3)_3$ electrolytes, respectively, after 600 charge-discharge cycles. The factors influencing cycle-life of MnO_2 electrodes are not understood, corrosion of the substrate metal could be a possibility.[20] It is interesting to note that SC measured in $La(NO_3)_3$ electrolyte is greater than the SC values measured in $Mg(NO_3)_2$ and $NaNO_3$ electrolytes throughout the cycle-life test (Fig. 11).

Conclusions

It has been shown that MnO_2 exhibits superior supercapacitor behaviour in $La(NO_3)_3$ electrolyte in comparison with $Mg(NO_3)_2$ and $NaNO_3$ electrolytes. The specific capacitance increases with an increase in charge present on the cation of the electrolyte. It is proposed that insertion of the trivalent cation, La^{3+} on the surface of MnO_2 particles leads to an increase in Mn^{4+} ions undergoing reduction to Mn^{3+} ions.

References

1. F. Jiao and P. G. Bruce, *Adv. Mater.*, **19**, 657 (2007).
2. D. Liu, Q. Zhang, P. Xiao, B. B. Garcia, Q. Guo, R. Champion, and G. Cao, *Chem. Mater.*, **20**, 1376 (2008).
3. Y. Yang, L. Xiao, Y. Zhao, and F. Wang, *Int. J. Electrochem. Sci.*, **3**, 67 (2008).
4. H. Y. Lee and J. B. Goodenough, *J. Solid State Chem.*, **144**, 220 (1999).
5. C. C. Hu and T. W. Tsou, *Electrochem. Commun.*, **4**, 105 (2002).
6. S. L. Kuo and N. L. Wu, *J. Electrochem. Soc.*, **153**, A1317 (2006).
7. M. Toupin, T. Brousse, and D. Belanger, *Chem. Mater.*, **16**, 3184 (2004).
8. V. Subramanian, H. Zhu, and B. Wei, *J. Power Sources*, **159**, 361 (2006).
9. S. Devaraj and N. Munichandraiah, *J. Phys. Chem. C*, **112**, 4406 (2008).

10. C. C. Hu, C. Y. Hung, K. H. Chang, and Y. L. Yang, *J. Power Sources*, **196**, 847 (2011).
11. P. Ragupathy, H. N. Vasan, and N. Munichandraiah, *J. Electrochem. Soc.*, **155**, A34 (2008).
12. C. C. Hu and C. C. Wang, *J. Electrochem. Soc.*, **150**, A1079 (2003).
13. R. Jiang, T. Huang, J. Liu, J. Zhuang, and A. Yu, *Electrochim. Acta*, **54**, 3047 (2009).
14. C. Xu, H. Du, B. Li, F. Kang, and Y. Zeng, *J. Electrochem. Soc.*, **156**, A73 (2009).
15. C. Xu, H. Du, B. Li, F. Kang, and Y. Zeng, *J. Electrochem. Soc.*, **156**, A435 (2009).
16. P. Ragupathy, D. H. Park, G. Campet, H. N. Vasan, S. J. Hwang, J. H. Choy, and N. Munichandraiah, *J. Phys. Chem. C*, **113**, 6303 (2009).
17. M. Wei, Y. Konishi, H. Zhou, H. Sugihara, and H. Arakawa, *Nanotechnology*, **16**, 245 (2005).
18. J. A. Dean, *Lange's Handbook of Chemistry*, McGraw-Hill, New York (1992).
19. D. Briggs and M. P. Seah, *Practical Surface Analysis by Auger and X-ray Photoelectron Spectroscopy*, John Wiley & Sons, New York (1983).
20. T. Brousse, P-L. Taberna, O. Crosnier, R. Dugas, P. Guillemet, Y. Scudeller, Y. Zhou, F. Favier, D. Belanger, and P. Simon, *J. Power Sources*, **173**, 633 (2007).